

Saturation wind power potential and its implications for wind energy

*Original*

Saturation wind power potential and its implications for wind energy / Jacobson, M. Z.; Lozej Archer, C.. - In: PROCEEDINGS OF THE NATIONAL ACADEMY OF SCIENCES OF THE UNITED STATES OF AMERICA. - ISSN 0027-8424. - 109:39(2012), pp. 15679-15684. [10.1073/pnas.1208993109]

*Availability:*

This version is available at: 11583/3009037 since: 2026-03-22T16:31:30Z

*Publisher:*

National Academy of Sciences

*Published*

DOI:10.1073/pnas.1208993109

*Terms of use:*

This article is made available under terms and conditions as specified in the corresponding bibliographic description in the repository

*Publisher copyright*

(Article begins on next page)

# 1 **Saturation Wind Power Potential and its Implications for Wind Energy**

2  
3 Mark Z. Jacobson<sup>1</sup>, Cristina L. Archer<sup>2</sup>

4  
5 (1) Department of Civil and Environmental Engineering, Stanford University, Stanford,  
6 California 94305-4020, USA; Email: [jacobson@stanford.edu](mailto:jacobson@stanford.edu); Tel: (650) 723-6836.

7 (2) Physical Ocean Science and Engineering, University of Delaware, Email:  
8 [carcher@udel.edu](mailto:carcher@udel.edu); Tel: (302) 831-6640.

## 9 10 11 Abstract

12 Wind turbines convert kinetic to electrical energy, which returns to the atmosphere as  
13 heat to regenerate some potential and kinetic energy. As the number of wind turbines  
14 increases over large geographic regions, power extraction first increases linearly, but then  
15 converges to a saturation potential not identified previously from physical principles or  
16 turbine properties. These saturation potentials are ~255 TW at 100 m globally, ~80 TW at  
17 100 m over land plus coastal ocean outside Antarctica, and ~380 TW at 10 km in the jet  
18 streams. Thus, there is no fundamental barrier to obtaining half (~5.75 TW) or several  
19 times the world's all-purpose power from wind in a 2030 clean-energy economy.

## 20 21 Introduction

22 A new method is proposed to determine the maximum theoretical wind power potential  
23 on Earth, based on the concept of “saturation”. The *saturation wind power potential*  
24 (SWPP) is the maximum wind power that can be extracted upon increasing the number of  
25 wind turbines over a large geographic region, independent of societal, environmental,  
26 climatic, or economic considerations. Once the SWPP is reached, increasing the number  
27 of turbines further does not increase the generated power further. At the SWPP, winds  
28 still occur because individual turbines can extract no more than 59.3 percent of the  
29 kinetic energy in the wind (Betz's limit). This paper also defines the *fixed wind power*

1 *potential* (FWPP), which is the maximum power that can be extracted by a fixed number  
2 of wind turbines at decreasing installed density and increasing geographic area. The  
3 SWPP is calculated here at 100 m hub height above ground assuming conventional wind  
4 turbines distributed everywhere on Earth, including over the oceans (simulation named  
5 “global-SWPP”) and, separately, over land only but excluding Antarctica (“land-SWPP”).  
6 The SWPP is also calculated at 10 km above ground in the jet streams assuming Airborne  
7 Wind Energy devices (“global-SWPP”). Capturing jet stream winds presents greater  
8 technological challenges than capturing surface winds but is still of interest (1, 2).

9         The main purpose of these simulations is to use a physical model to determine the  
10 theoretical limit of wind energy available at these altitudes, particularly since some recent  
11 studies that accounted for energy extraction by turbines, but not physically, have  
12 suggested that available wind energy is small (2, 3). Previous theoretical estimates of the  
13 power in the wind (4-9) are similarly not based on a physical model of energy extraction  
14 so cannot give estimates of wind potential at the height of turbines. As found here, energy  
15 extraction at a given altitude does not deplete energy at all altitudes above or below it; so  
16 an estimate of wind potential in the whole atmosphere does not answer the practical  
17 question about wind turbine potential at typical hub heights.

18         More relevant for practical applications, the FWPP of 4 million turbines at 100 m  
19 in three different configurations is quantified here to determine if this number is  
20 sufficient for powering half the world’s all-purpose power demand in a 2030 clean-  
21 energy economy (10).

22         It is well known that the array efficiency of a single wind or water farm  
23 containing many turbines decreases with decreasing distance between turbines (11, 12).  
24 However, what is not known is the extent to which the efficiency loss operates globally  
25 when realistic meteorology and energy extraction by turbines are accounted for. This  
26 information is critical for determining the feasibility of worldwide renewable energy  
27 future. Calculating the SWPP for large penetrations of wind ( $\geq 1$  TW) is not currently

1 possible from data analysis, since penetrations are still low (239 GW installed worldwide  
2 as of 2012). The most accurate method available to analyze this issue is with a complex  
3 3-D atmospheric-ocean-land coupled model.

4 Previous global simulations of wind farms have assumed that wind farm effects  
5 on the atmosphere can be represented by changing surface roughness or adding a drag  
6 coefficient (2, 3, 13-17). Roughness parameterizations, though, incorrectly reduce wind  
7 speeds the most in the bottom model layer, whereas in reality a surface wind turbine  
8 reduces wind speed the most at hub height, ~100 m above ground (Fig. 1). Since  
9 roughness lengths and drag coefficients are approximate, it is also difficult to ensure they  
10 extract the correct amount of energy from the wind. *Calaf et al. (18)* demonstrated the  
11 inaccuracy of standard roughness parameterizations against large-eddy simulation results  
12 and developed a multiple-layer roughness parameterization for ground-based turbines  
13 that is more accurate. Here, however, we use a straightforward approach to calculate the  
14 momentum sink at any specified hub height, not just near the ground, but also aloft, each  
15 time step, since it precisely determines the time-dependent energy extraction from one or  
16 many turbines.

17 Another common omission during modeling has been that of energy conservation  
18 during electric power use and turbulence dissipation. If wind turbines generate 5.75 TW  
19 ( $0.0113 \text{ W/m}^2$ ), such power ultimately returns to the air as heat following electricity use.  
20 This heat does not depend on the electricity source, thus it is also released when coal,  
21 nuclear, and gas produce electricity. Such generators, though, produce additional heat due  
22 to combustion or nuclear reaction and emit global warming pollutants (19, 10). As such,  
23 wind turbines reduce direct heat and pollutant emissions compared with conventional  
24 generators. However, the electricity use still needs to be accounted for since it is a source  
25 of some regenerated kinetic energy (via conversion of internal energy to some available  
26 potential energy to kinetic energy). To date, only (1) has calculated the heat from

1 electricity returned to the air, but they focused on airborne rather than ground-based wind  
2 turbines.

3

#### 4 Model Treatment of Wind Turbine Energy Extraction

5 Here, the GATOR-GCMOM global model (20, 21) is used to examine saturation and  
6 fixed wind power potentials. The model is modified to treat wind turbines as an elevated  
7 momentum sink, where the kinetic energy extracted from the wind is determined from a  
8 turbine power curve at the instantaneous model wind speed. The treatment of turbines  
9 developed is conceptually similar to that in (22, 23) but differs as follows: it (1) assumes  
10 each wind turbine occupies multiple vertical atmospheric layers rather than one layer, (2)  
11 extracts energy from momentum points on an Arakawa C grid rather than from the center  
12 of the cell, (3) is applied to numerous wind farms worldwide simultaneously rather than  
13 one local farm, (4) is applied in a global model where momentum extraction feeds back  
14 to global dynamics rather than a limited-area model with only regional feedbacks, and (5)  
15 accounts for energy conservation due to both electricity use and turbulent dissipation of  
16 kinetic energy.

17 The Supporting Text (24) describes the model treatment of wind turbine kinetic  
18 energy extraction. Briefly, each turbine is characterized by a rated power ( $P_r$ , 5 MW),  
19 rotor diameter ( $D$ , 126 m), hub height above the topographical surface ( $H$ , 100 m or 10  
20 km), and characteristic spacing area ( $A_r$ ,  $m^2$ ) each simulation. Each turbine is assumed to  
21 intersect multiple atmospheric layers of a grid column (Fig. S1). Each time step, kinetic  
22 energy is extracted from each model layer that intersects the turbine rotor. The kinetic  
23 energy reduction is translated into a wind speed reduction. The resulting shear produces  
24 turbulence. Energy is conserved by converting all electric power generated by the wind  
25 turbines to heat via electricity use at the surface, where it occurs, and by converting  
26 kinetic energy lost by natural surface roughness to turbulence, then heat.

27

1 Model Simulations

2 Table 1 summarizes the simulations. A control simulation (A) was first run with turbines  
3 at 100 m hub height but no momentum extraction from them. Figure S2 compares  
4 resulting near-surface wind speeds with data. To determine the global-SWPP at 100m,  
5 five  $4^\circ \times 5^\circ$  horizontal resolution sensitivity simulations (B-F) with momentum extraction,  
6 each with decreasing installed power density, were run. Simulations (G) ( $2.5^\circ \times 2.5^\circ$ ) and  
7 (H) ( $1.5^\circ \times 1.5^\circ$ ), comparable with (C), were then run to scale the coarse-resolution results  
8 to finer resolution.

9 To determine the land-SWPP (land excluding Antarctica) at 100 m, four  $4^\circ \times 5^\circ$   
10 simulations (I-L), each with decreasing power density, were run. A  $1.5^\circ \times 1.5^\circ$  simulation  
11 (M) was then run to scale results to finer resolution.

12 To determine the FWPP of 4 million 5-MW turbines, the number estimated to  
13 supply half the world's all-purpose power in a clean energy economy in 2030 (9), the  
14 turbines were distributed in three configurations: over all land 15S-60S and 15N-66.56N,  
15 and below 3 km altitude (Simulation N); over 8 land and coastal sites (Table 1, footnote)  
16 (O); and over 3 land sites (Table 1, footnote) (P).

17 Finally, to determine the SWPP of the jet streams (10-70N and 10-70S) at 10 km,  
18 a  $4^\circ \times 5^\circ$  simulation (Q) with the maximum power density as in simulation (B) was run. A  
19  $1.5^\circ \times 1.5^\circ$  simulation (R) was also run to scale results with resolution.

20 All simulations included 68 vertical sigma-pressure layers up to 0.219 hPa ( $\approx 60$   
21 km), including 15 layers from 0-1 km and 500-m resolution from 1-21 km. The center of  
22 the lowest model layer was 15 m above ground. The rotor of each surface turbine  
23 (simulations B-P) intersected five model layers. That of each jet-stream turbine  
24 (simulations Q-R) intersected two layers. The model was run forward from January 1,  
25 2006 with no data assimilation. Because this study does not focus on temperature  
26 response and due to the long computer time required for radiative, cloud, aerosol, and gas

1 processes, only five-year simulations were run. Wind power extraction in all five years  
2 was similar and convergent in all simulations.

3

#### 4 Results

5 Figure 2a shows that, up to about 715 TW ( $1.4 \text{ W/m}^2$ ) of installed power, the output from  
6 power-extracting wind turbines first increases linearly. The linearity is demonstrated by  
7 comparing the initial slope of the “global-SWPP curve” (with power extraction) with the  
8 slope of the “global-no power extraction” line. The latter is the line between zero and the  
9 power output from Simulation A, which is the reference case with turbines but without  
10 momentum extraction. At higher penetrations, power output increases with diminishing  
11 returns until it reaches global saturation ( $\sim 253 \text{ TW}$ , also Fig. S3b for coarse-resolution  
12 results) at about 2870 TW ( $5.65 \text{ W/m}^2$ ) installed. Higher penetrations of wind serve no  
13 additional benefit. Thus, for the first 715 TW installed, output increases roughly linearly  
14 proportionally to turbine installation, but thereafter, it increases with diminishing returns  
15 until saturation.

16 The global SWPP obtained in Fig. 2a is likely a lower bound since power  
17 extraction increases, while still converging, upon grid refinement. For example,  $1.5^\circ \times 1.5^\circ$   
18 resolution results (Simulation H) were about 1% higher than those at  $2^\circ \times 2.5^\circ$  (Simulation  
19 G), which were about 10% higher than at  $4^\circ \times 5^\circ$  (Simulation C). Even higher resolution  
20 may increase power output more (25).

21 The 253 TW of worldwide extractable power at 100 m is  $\sim 22.5$  times that of a  
22 simple-equation estimate of extractable power in the bottom 200 m of the atmosphere  
23 worldwide, 11.25 TW (3), calculated as the estimated total power in that region (100  
24 TW) multiplied by the fraction that could interact with wind turbine rotors ( $< 0.3$ ), the  
25 fraction in the range of turbine cut-in and cut-out speeds (0.75), and the fraction  
26 converted from kinetic to electrical energy (0.5). These factors were all accounted for in

1 time and space in the simulations here. The large difference highlights the importance of  
2 using physical calculations.

3 The SWPP over land outside Antarctica here was  $\sim 72$  TW (Fig. 2a, Fig. S3c).  
4 Based on the high-resolution global-SWPP calculations here, another  $\sim 8$  TW was  
5 available offshore at depths  $< 200$  m, giving a land plus coastal SWPP estimate of 80 TW.  
6 Like with the global case, the land-SWPP curve (Fig. 2a) shows a linear portion at low  
7 turbine penetrations. Beyond  $\sim 185$  TW of installed power, diminishing returns set in.  
8 However, the full land-SWPP was not obtained until  $\sim 1500$  TW ( $11.3 \text{ W/m}^2$ ) of installed  
9 power. The result here suggests that bottom-up approaches for calculating wind power  
10 potentials over land are justified for  $< 185$  TW installed power.

11 The land-SWPP is not much lower than the 125 TW of onshore power from a  
12 study (26) that assumed a fixed percentage energy loss due to turbine interference but not  
13 increasing competition for wind with increasing turbine penetration. Their result falls  
14 near the linear “global-no extraction” curve in Fig. 2a, just above the land-SWPP.

15 Another study (27) estimated the world land plus coastal wind potential based on  
16 world sounding and surface data as 72 TW. Similarly, (26) estimated a land potential of  
17 78 TW for capacity factors of 20% or higher. Both studies accounted only for locations  
18 with mean-annual wind speeds before extraction  $> 7$  m/s and did not account for  
19 increasing competition. These two offsetting factors caused their results to be similar to  
20 the land-SWPP (72 TW) and the land plus near-shore estimate ( $\sim 80$  TW) found here.

21 If only 50% of land-based wind were in economically-viable locations (3), the  
22 feasible wind potential on land (not counting near shore) here would be  $\sim 36$  TW, 36  
23 times the single-equation estimate from (3).

24 The SWPP at 10 km in the jet streams ( $\sim 378$  TW – Table 1, Fig. S3g) was  $\sim 150\%$   
25 that at 100 m despite fewer turbines in the jet stream case. The maximum jet stream  
26 power availability was  $\sim 50$  times that of a 7.5 TW estimate from (2), who used a global  
27 model with only 10 vertical layers to minimize computer time (versus 68 layers here) and

1 an elevated drag coefficient rather than extracting momentum based on a turbine power  
2 curve. The difference again highlights the importance of calculating the SWPP from  
3 physical principles. SWPPs are extractable energy potentials, not just available energy  
4 potentials, thus include losses and efficiencies. Airborne jet-stream turbines would  
5 require energy to ascend and descend and may not operate all year. This analysis does not  
6 quantify such losses, only extractable energy.

7         The extractable power globally at 100 m and, separately, at 10 km in the jet  
8 streams, are both independently less than the total extractable power in the wind at all  
9 altitudes, estimated broadly as 450-3800 TW (4-9). These previous studies, though, did  
10 not consider extraction at a single altitude, such as the height of modern wind turbines  
11 nor did they use a 3-D model to make their estimates. Extraction of power at each 100 m  
12 and at 10 km does not give the same dissipation as complete extraction of kinetic energy  
13 from the atmosphere, as seen in Figure 1; instead, each results in wind reduction over a  
14 vertical segment of the atmosphere, decreasing with distance from the height of  
15 extraction.

16         Simulations N-P examine whether ~4 million 5-MW turbines (20 TW installed)  
17 can provide at least 5.75 TW of delivered power, enough to supply 50% of all-purpose  
18 end-use power demand in 2030 for a world energy infrastructure converted to wind,  
19 water, and sunlight (WWS) and electricity/hydrogen (10). Figure 2b shows that the power  
20 output of 4 million turbines increases with decreasing wind turbine spacing. When  
21 turbines are packed at an installed density of 11.3 W/m<sup>2</sup> into 3 sites worldwide, the power  
22 output is too low (~1.6 TW – Table 1, Fig. S3f) to match power demand. At 8 locations  
23 (5.6 W/m<sup>2</sup> installed), the output improves to ~4 TW (Fig. S3e) but is still lower than  
24 needed. However, when turbines are spread over land outside the tropics, away from the  
25 poles, and in all regions below 3 km altitude (0.11 W/m<sup>2</sup> installed), the output jumps to  
26 ~7.5 TW (Fig. S3d), much more than needed. The crossover point is at an installed  
27 density of ~2.9 W/m<sup>2</sup>. It is not necessary to spread turbines evenly across such land. In

1 fact, individual farms can have installed densities of 5.6-11.3 W/m<sup>2</sup> so long as reasonable  
2 spreading between farms occurs and the average installed density within and between  
3 farms is  $\leq 2.9$  W/m<sup>2</sup> (or  $\leq 3.1$  W/m<sup>2</sup> accounting for higher model resolution).

4 It is well known that spreading wind turbines in a farm increases farm array  
5 efficiency by decreasing interference of one turbine with the next (11, 12). The results  
6 here suggest that staggering farms themselves, geographically, improves the overall  
7 power output. In other words, the power potential of a fixed number of turbines (FWPP)  
8 increases with increased spreading of farms.

9 The addition of surface wind turbines reduced horizontal wind speeds in their  
10 wake the most and below and above the wake centerline to a lesser extent (Figure 1a).  
11 The reduction in wake wind speed reduced shearing stress below and increased it above  
12 the wake centerline, consistent with large-eddy-simulation results (18). Greater shearing  
13 stress above the wake increased turbulent kinetic energy (TKE) there, increasing the  
14 downward flow of horizontal momentum from above to the turbines. Lesser shearing  
15 stress below the wake decreased TKE and downward momentum fluxes near the surface.  
16 Evaporation rates are proportional to both surface wind speeds and surface shearing stress,  
17 and both decreased in all surface turbine simulations, reducing evaporation and water  
18 vapor (e.g., Fig. 1c). These calculations were all made with the model resolving the  
19 bottom kilometer with 15 vertical layers, including 5 layers intersecting turbine rotors.

20 Drag from blade rotation also creates turbulence in the form of small-scale  
21 vortices that can enhance vertical mixing. This mechanism has been suggested by (28) to  
22 explain why wind turbines decrease downwind surface temperatures during the day,  
23 when the lapse rate is generally unstable, and slightly increase them at night, when the  
24 lapse rate is generally stable. While this effect may sometimes play a role, turbulent  
25 wakes generally spread out and dissipate horizontally rather than vertically downwind in  
26 the wake of a turbine (18), and therefore the wake turbulence remains elevated and rarely  
27 reaches the ground. Even when wake turbulence reaches the ground, it is largely offset by

1 reduced turbulent shear due to the reduced wind speed in the wake and thus the reduced  
2 shearing stress below the turbine. We propose here that wind turbines, on average, reduce,  
3 rather than enhance, turbulence near the ground because of the reduced shearing stress.  
4 Both the reduced wind speed and reduced shearing stress near the surface contributed to  
5 reducing surface evaporation.

6 Reduced evaporation reduced evaporative cooling of the surface, first warming  
7 the surface. However, because evaporated water vapor normally recondenses in the  
8 atmosphere to form clouds, releasing latent heat there, the reduction in water vapor  
9 reduced latent heat release in the air, cooling the air due to this process. Because water  
10 vapor contributes to air pressure, reducing water vapor also reduced globally-averaged air  
11 pressure by  $\sim 0.3$  and  $\sim 0.1$  hPa in the global (Simulation B) and land (I) cases,  
12 respectively. Since water vapor is a greenhouse gas, reducing it increased thermal-IR  
13 radiation escape to space, cooling the surface further. However, less water also reduced  
14 cloudiness, increasing solar radiation to the surface during the day but increasing  
15 outgoing thermal-IR at night, thus causing a slight warming at night, as observed (28, 29).  
16 The net effect of all five changes (air cooling due to lower atmospheric latent heat release,  
17 ground warming due to lower surface water evaporation, air and ground cooling due to a  
18 reduced water vapor greenhouse effect, ground warming due to reduced daytime  
19 cloudiness, and ground cooling due to reduced nighttime cloudiness) was a globally-  
20 averaged surface-air temperature decrease in 15 out of the 16 surface-turbine simulations.  
21 This is expected since water vapor is known to cause net warming of the atmosphere, so  
22 reducing it should cause cooling (30). Temperature results, though, are still uncertain,  
23 particularly due to the uncertainty of clouds and the transient nature of the simulations  
24 and could change over longer simulations since full temperature responses take decades  
25 to realize. A certain benefit of the slower winds, though, is the reduction in wind-driven  
26 soil dust; sea spray; and spore, pollen, and bacteria emissions, reducing human exposure  
27 to small particles that penetrate deep into the lungs.

1 Globally-distributed turbines decreased zonal winds; however, they increased  
2 meridional winds in the poleward direction in both hemispheres (Figs. S4a,b). The  
3 poleward transport of air increased the pressure gradient between the poles and Equator  
4 by  $\sim 15\text{-}25$  hPa, supporting the contention that the atmosphere responded to the increased  
5 dissipation of kinetic energy by increasing some of its available potential energy via  
6 enhanced pole-to-Equator pressure gradients. Reduced water vapor partial pressure at low  
7 latitudes contributed to the enhanced pressure gradient.

8 Jet-stream turbines reduced mean wind speeds at altitudes above and below them,  
9 but increased boundary-layer wind speeds (Fig. 1c). Like in the surface case, turbines  
10 decreased zonal wind speeds substantially (Fig. S5a), but increased meridional wind  
11 speeds (Fig. S5b), moving air poleward at 10 km but equatorward near the surface in both  
12 hemispheres, following the respective pressure gradients (Fig. S5c). Lower surface  
13 pressure in the tropics through midlatitudes caused air to rise, expand, and cool  
14 adiabatically, decreasing temperatures at all altitudes (Fig. S5d) and increasing both  
15 cloud liquid below 5 km (Fig. S5e) and cloud ice above that. Enhanced cloudiness  
16 increased precipitation, and both, together with net divergence, decreased water vapor in  
17 the tropics and subtropics and increased it toward the poles (Fig. S5f). Compressional  
18 heating over the poles increased temperatures there, but the net effect of jet stream  
19 turbines was surface cooling by  $>1$  K (Fig. S5f), as cold air advection from the Poles  
20 prevailed near the surface. Interestingly, the higher boundary-layer wind speeds (Figs. 1c,  
21 S5a) increased evaporation there, but enhanced condensation of that vapor decreased  
22 column vapor at low latitudes (Fig. S5f).

23 The results here suggest that saturation of wind power availability will not limit a  
24 clean-energy economy. However, spreading wind farms out worldwide in high-wind  
25 locations will increase wind farm efficiency and reduce the number of farms needed  
26 compared with packing wind farms side-by-side. The careful siting of wind farms will

1 minimize costs and the overall impacts of a global wind infrastructure on the  
2 environment.

3 Acknowledgements. Funding sources include NSF, U.S. EPA, and NASA high-end  
4 computing.

5

#### 6 References and Notes

- 7 1. Archer, C.L. & Caldeira K. (2009) *Energies* **2**, 307-319.
- 8 2. Miller, L.M., Gans, F. & Kleidon, A. (2011) *Earth Syst. Dynam.* **2**, 201-212.
- 9 3. De Castro, C., Mediavilla, M., Miguel, L. J. & Frechoso F. (2011) *Energy Policy* **39**,  
10 6677-6682.
- 11 4. Lorenz, E.N. (1967) *The nature and theory of the general circulation of the*  
12 *atmosphere*. WMO, Geneva, 161 pp.
- 13 5. Gustavson, M.R. (1979) *Science* **204**, 13-17.
- 14 6. Peixoto, J.P. & Oort, A. H. (1992), *Physics of climate*, American Institute of Physics,  
15 520 pp..
- 16 7. Sorensen, B. (2004) *Renewable Energy: Its Physics, Engineering, Use,*  
17 *Environmental Impacts, Economy, and Planning Aspects*, Third Edition, Elsevier  
18 Academic Press, London.
- 19 8. Li, L., Ingersoll, A.P., Jiang, X., Feldman, D. & Yung Y.L. (2007), *Geophys. Res.*  
20 *Lett.* **34**, L16813.
- 21 9. Stacey, F. D. & Davis, P. M. (2008) *Physics of the Earth*, Fourth Edition, Cambridge  
22 University Press, 531 pp..
- 23 10. Jacobson, M.Z. & Delucchi M.A. (2011), *Energy Policy* **39**, 1154-1169.
- 24 11. Milborrow, D.J. (1980) *J. Wind Eng. Ind. Aerodynamics* **5**, 403-430.
- 25 12. Li, Y. & Calisal, S.M. (2010) *Intl. J. Green Energy* **7**, 153-163.
- 26 13. Keith, D.W., DeCarolis, J.F., Denkenberger, D.C. et al. (2004) *Proc. Natl. Acad. Sci.*  
27 **101**, 16,115-16,120.
- 28 14. Kirk-Davidoff, D.B. & Keith D. (2008) On the climate impact of surface roughness  
29 anomalies, *J. Atmos. Sci.* **85**, 2215-2234.
- 30 15. Barrie, D. & Kirk-Davidoff D.B. (2010) *Atmos. Chem. Phys.* **10**, 769-775.
- 31 16. Wang, C. & Prinn, R.J. (2010) *Atmos. Chem. Phys.* **10**, 2053-2061.
- 32 17. Miller, L.M., Gans, F. & Kleidon A. (2011) *Earth Syst. Dynam.* **2**, 1-12.
- 33 18. Calaf, M., Meneyeau, C. & Meyers, J. (2010) *Physics of Fluids* **22**, 015110.
- 34 19. Sta. Maria, M.R.V. & Jacobson, M.Z. (2009) *Energies* **2**, 816-836..
- 35 20. Jacobson, M.Z., Wilkerson, J.T., Naiman, A.D. & Lele, S.K. (2011) *J. Comp. Phys.*  
36 **230**, 5115-5132.
- 37 21. Jacobson, M.Z. & Ten Hoeve, J.E. (2012) *J. Climate* **25**, 1028-1044.
- 38 22. Baidya Roy, S., Pacala, S.W. & Walko, R.I. (2004) *J. Geophys. Res.* **109**, D19101.
- 39 23. Baidya Roy, S. (2011) *J. Wind Eng. Ind. Aerodyn.* **99**, 491-498..
- 40 24. Materials and methods are available as supporting material on Science Online.
- 41 25. Pryor, S.C., Nikulin, G. & Jones C. (2012) *J. Geophys. Res.* **117**, D03117.
- 42 26. Lu, X., McElroy, M. & Kiviluoma, J. (2009) *P. Natl. Acad. Sci.* **106**, 10,933-10,938.
- 43 27. Archer, C.L. & Jacobson M.Z. (2005) *J. Geophys. Res.* **110**, D12110.

- 1 28. Baidya Roy, S. & J. J. Traiteur (2010), *Proc. Nat. Acad. Sci.*, 107(42), 17899–17904,  
2 doi:10.1073/pnas.1000493107.
- 3 29. Zhou, L., Tian, Y., Baidya Roy, S., Thorncroft, C., Bosart, L.F. & Yuanlong, H.  
4 (2012) *Nature Climate Change*, doi:10.1038/nclimate1505.
- 5 30. Kiehl, J.T. & Trenberth, K.E. (1997) Earth's annual global mean energy budget, *Bull.*  
6 *Amer. Met. Soc.* **78**, 197-208.
- 7 31. Lettau, H. (1969) *J. Appl. Meteorol.* **8**, 828-832.
- 8
- 9

Table 1. Summary of Simulations and Power Output in Year 5

Simulation	Model Horizontal Resolution (degrees)	Turbine Spacing $A_r$ (m <sup>2</sup> )	Total Number of 5-MW Turbines (millions)	Number of Turbines Over Ocean (millions)	Total Installed Power (TW)	Percent of World for Spacing	Turbine Installed Power Density (W/m <sup>2</sup> )	Annual Total Power Output Year 5 (TW)
Global-SWPP								
A) World (control)	4x5	28D <sup>2</sup>	1146	821	5730	100	11.3	1750
B) World	4x5	28D <sup>2</sup>	1146	821	5730	100	11.3	224
C) World	4x5	56D <sup>2</sup>	573	411	2864	100	5.62	228
D) World	4x5	84D <sup>2</sup>	382	274	1909	100	3.75	219
E) World	4x5	112D <sup>2</sup>	286	205	1432	100	2.81	206
F) World	4x5	224D <sup>2</sup>	143	103	716	100	1.41	160
G) World	2x2.5	56D <sup>2</sup>	574	410	2870	100	5.65	<sup>f</sup> 251
H) World	1.5x1.5	56D <sup>2</sup>	575	410	2872	100	5.65	<sup>f</sup> <b>253</b>
<sup>g</sup> Land-SWPP								
I) Land	4x5	28D <sup>2</sup>	299	0	1495	26.0	11.3	71.2
J) Land	4x5	56D <sup>2</sup>	149	0	747.6	26.0	5.62	66.7
K) Land	4x5	112D <sup>2</sup>	74.8	0	373.8	26.0	2.81	56.4
L) Land	4x5	224D <sup>2</sup>	37.4	0	186.9	26.0	1.41	39.7
M) Land	1.5x1.5	28D <sup>2</sup>	302	0	1510	26.3	11.3	<sup>f</sup> <b>72.0</b>
Land-FWPP								
N) <sup>b</sup> Land	4x5	1470D <sup>2</sup>	4	0	20	18.3	0.21	<b>7.50</b>
O) <sup>c</sup> Land+coast 8 sites	4x5	56D <sup>2</sup>	4	0.004	20.195	0.696	5.62	<b>3.93</b>
P) <sup>d</sup> Land 3 sites	4x5	28D <sup>2</sup>	4	0	20.105	0.348	11.3	<b>1.63</b>
Jet stream-SWPP								
Q) <sup>e</sup> Jet stream	4x5	28D <sup>2</sup>	931	668	4653	81.0	11.3	375
R) <sup>e</sup> Jet stream	1.5x1.5	28D <sup>2</sup>	941	673	4707	81.9	11.3	<sup>f</sup> <b>378</b>

Earth's surface area is 510.6 million km<sup>2</sup>. Hub heights were 100 m above ground level except in the jet stream cases (10 km).  $D=126$  m is turbine rotor diameter.

<sup>g</sup>Land in these cases included all land north of 60S (outside of Antarctica) but did not include coastal ocean.

<sup>b</sup>Land in this case included all land 15S-60S, 15N-66.56083N (Arctic Circle), and below 3 km but did not include coastal ocean.

<sup>c</sup>All turbines in this case were distributed among 19 windy cells in 8 locations, the Great Plains (4 cells), offshore East Coast (3), North Sea (2), Sahara Desert (3), Gobi Desert (2), Yellow Sea (1), Australia (2), and Patagonia (2).

<sup>d</sup>All turbines in this case were distributed among 9 windy cells in 3 locations, the Great Plains (4 cells), Sahara Desert (3), and Gobi Desert (2).

<sup>e</sup>The jet stream winds considered were 10S-70S, 10N-70N, and at 10 km altitude. Top and bottom turbine heights were 10.063 km and 9.937 km, respectively.

<sup>f</sup>The  $1.5^{\circ} \times 1.5^{\circ}$  simulations were run for only six months and the  $2^{\circ} \times 2.5^{\circ}$  simulations, for one year, due to their enormous computing requirements. The ratio of the power generation averaged over the months or year to that from the same time for the corresponding  $4^{\circ} \times 5^{\circ}$  resolution simulation was multiplied by the last-year annual-average result from the  $4^{\circ} \times 5^{\circ}$  simulation to estimate the  $1.5^{\circ} \times 1.5^{\circ}$  and  $2^{\circ} \times 2.5^{\circ}$  power generation averaged over the last year for conditions from that simulation.

**Figure 1.** Comparison of heights and magnitudes of globally-averaged percent wind speed reduction averaged over one year from (a) the turbine momentum sink parameterization presented here versus (b) the Lettau (31) surface roughness parameterizations. In both cases, the world is covered with either 1.146 billion, 324.5 million, or 4 million 5-MW, 126-m rotor diameter turbines with hub height of 100 m, spaced  $0.44 \text{ km}^2$  each. In (a), a jet stream case is also shown for 931 million 5-MW turbines with hub height at 10 km. (c) Percent difference in water vapor mass mixing ratio vertical profiles between the world (Simulation B), land (I), and jet stream (Q) cases and the base case (A). All these simulations were run at  $4^\circ \times 5^\circ$  horizontal resolution.

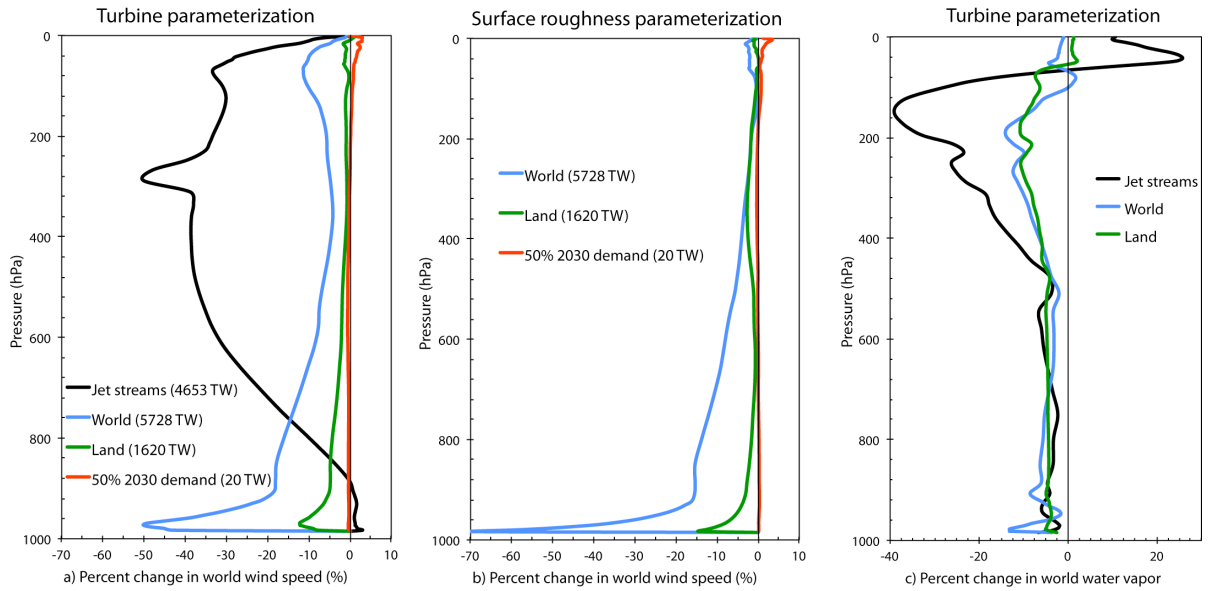
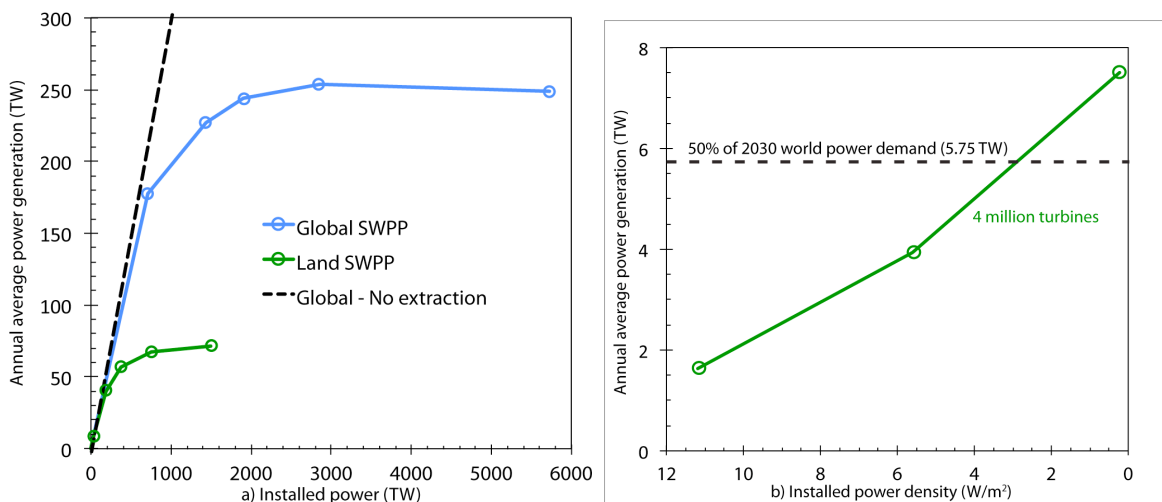


**Figure 2.** (a) Convergence to global-SWPP (Simulations B-F) and land-SWPP outside Antarctica (Simulations I-L and N) scaled by higher-resolution results from Simulations H and M, respectively. As such, values represent  $4^\circ \times 5^\circ$  results from Table 1 scaled by  $1.5^\circ \times 1.5^\circ$  results, from the table. Also shown is the straight line between 0 and 1750 TW power output (at 5730 TW, or  $11.3 \text{ W/m}^2$ , installed power) from the global turbine, no-power-extraction case (Simulation A). The highest installed turbine density in the land-SWPP case was also  $11.3 \text{ W/m}^2$ . (b) Wind power potential at three installed power densities of 4 million wind turbines. Also shown is 50% of the world all-purpose power demand in 2030 upon conversion to wind, water, and sunlight (WWS) and electricity/electrolytic hydrogen.



## **Saturation Wind Power Potential and its Implications for Wind Energy**

Mark Z. Jacobson, Cristina L. Archer

### **This PDF file includes:**

Supporting Materials and Methods

Supporting Figs. S1 to S3

Supporting References and Notes (S1-S5)

### **Supporting Materials and Methods**

The model used for this study was GATOR-GCMOM, a global-through-urban nested model (SI, 20, 21). The model was modified to treat wind turbines as an elevated sink of momentum, where the kinetic energy extracted from the wind is determined from a turbine power curve at the instantaneous model wind speed. The treatment of turbines developed here is similar in concept to that of *Baidya Roy* (22, 23) but differs in the following ways: it (1) assumes each wind turbine occupies multiple vertical atmospheric layers rather than one layer, (2) extracts energy from momentum points on an Arakawa C grid rather than from the center of the cell, (3) is applied to numerous wind farms worldwide simultaneously rather than one local farm, (4) is applied in a global model where momentum extraction feeds back to global dynamics rather than a limited-area model with only regional feedbacks, and (5) accounts for the conservation of energy due to both electricity use and turbulent dissipation of kinetic energy. In addition, the model adjusts winds on a staggered Arakawa C grid rather than a grid with centralized  $u$ , and  $v$  values.

The treatment of kinetic energy extraction by wind turbines in the model is described as follows. Each turbine is characterized by a rated power ( $P_r$ , 5 MW), a rotor diameter ( $D$ , 126 m), a hub height above the topographical surface ( $H$ , 100 m), and a characteristic spacing area ( $m^2$ )  $A_t = xD \times yD$ , usually determined by convention to minimize interference of the wake of one turbine with the next. In this equation,  $x$  and  $y$  are constants that provide distances perpendicular

to and parallel to, respectively, the prevailing wind direction. Some values used previously have been  $x=4, y=7; x=3, y=10$  (S2).

Each model grid cell contains a specified number of turbines. The maximum number of turbines in the grid cell is  $N_t=A_c/A_r$ , where  $A_c$  is the ground area occupied by the cell ( $m^2$ ).

For determining extraction of energy, each turbine is assumed to intersect one or more atmospheric layers of a grid column. This configuration applies regardless of whether the turbines exist in the boundary layer or jet stream and for either global or regional domains. The configuration requires modification only when the horizontal resolution of the model  $< D=126$  m in the present application. All simulations here are at coarser horizontal resolution than this.

The momentum extracted from each layer  $k$  that the turbine intersects is proportional to the ratio of the swept area of the turbine residing in the layer ( $S_k$ ) divided by the total swept area ( $m^2$ ) of the turbine,  $S_t=\pi D^2/4$ . The swept area residing in a layer is determined from geometry. For example, the swept area falling in the lowest layer of Figure S1 (ABCD) is the area HADCH minus the area HABCH. Since the hub height (point H) and the height above the ground of the edge of each layer (e.g., point B) are known, the vertical distance HB is also known. Since the distance HC, which is the turbine radius  $R=D/2$ , is also known, the angle BHC is  $\theta_{BHC}=\arccos(HB/R)$ . Therefore, area HADCH= $2\theta_{BHC}S_t/2\pi$ , and area HABCH= $HB \times R\sin(\theta_{BHC})$ . The areas of subsequent layers are calculated from bottom to top in a similar manner, taking into account the summed areas determined already.

Kinetic energy is extracted from each model layer that intersects the turbine rotor each time step  $\Delta t$  due to conversion of the kinetic energy to electric power by the turbine. The global and regional domains in the model use the Arakawa C grid structure; thus,  $u$  scalar velocities are located at the west ( $i-1/2, j$ ) and east ( $i+1/2, j$ ) edges of each grid cell in each layer  $k$ ,  $v$  scalar velocities are located at the south ( $i, j-1/2$ ) and north ( $i, j+1/2$ ) edges, and mass  $M$  (kg) and other scalars are located at the center ( $i, j, k$ ) of the cell. As such, the initial (subscript I) total kinetic energy in grid cell  $i, j, k$  before energy extraction is

$$E_{1,i,j,k} = 0.5 \left( E_{1,i-1/2,j,k} + E_{1,i+1/2,j,k} + E_{1,i,j-1/2,k} + E_{1,i,j+1/2,k} \right) \quad (S1)$$

In this equation,

$$\begin{aligned} E_{1,i-1/2,j,k} &= 0.5 M_{i-1/2,j,k} u_{1,i-1/2,j,k}^2 \quad \text{where} \quad M_{i-1/2,j,k} = 0.5 \left( M_{i-1,j,k} + M_{i,j,k} \right) \\ E_{1,i+1/2,j,k} &= 0.5 M_{i+1/2,j,k} u_{1,i+1/2,j,k}^2, \quad \text{where} \quad M_{i+1/2,j,k} = 0.5 \left( M_{i,j,k} + M_{i+1,j,k} \right) \\ E_{1,i,j-1/2,k} &= 0.5 M_{i,j-1/2,k} v_{1,i,j-1/2,k}^2, \quad \text{where} \quad M_{i,j-1/2,k} = 0.5 \left( M_{i,j-1,k} + M_{i,j,k} \right) \\ E_{1,i,j+1/2,k} &= 0.5 M_{i,j+1/2,k} v_{1,i,j+1/2,k}^2, \quad \text{where} \quad M_{i,j+1/2,k} = 0.5 \left( M_{i,j,k} + M_{i,j+1,k} \right) \end{aligned} \quad (S2)$$

The average horizontal wind speed at the vertical and horizontal center of a cell, used to determine kinetic energy extraction by a wind turbine to produce electricity, is thus  $W_{i,j,k} = [2E_{i,j,k}/M_{i,j,k}]^{1/2}$ . Each time step, the kinetic energy extracted from the turbine in a given cell is calculated as

$$\Delta E_{i,j,k} = P_{i,j,k} \Delta t S_k / S_t, \quad (S3)$$

where  $P_{i,j,k}$  is the power extracted from the turbine at instantaneous wind speed  $W_{i,j,k}$  based on its power curve. Equation S3 implies that the power determined from the power curve is calculated with a different wind speed in each model layer intersecting the turbine. Whereas power curves are derived based on the wind speed at hub height, the assumption of varying power extraction for varying heights in the turbine is necessary, since otherwise it would be possible to extract more energy from a layer than is physically present. For example, suppose (in a hypothetical extreme case), the wind speed were 0 m/s in the lowest layer intersecting the turbine and 10 m/s at hub height. Subtracting a portion of the total energy extracted from the lowest layer would be unphysical. Since wind speeds vary roughly logarithmically with height and the height of a turbine swept area is only  $D$ , higher wind power extracted at the turbine top are roughly compensated for by lower power extracted at the bottom. The error due to this assumption is likely less than the error due to that of the power curve, which is derived under neutrally-stratified conditions in the absence of wind shear.

For the RePower 5-MW turbine, a fit to the power curve data, combined with a correction for air density, is

$$P_{i,j,k} = \frac{\rho_a(T,P,q)}{\rho_{a,STP}} \begin{cases} 0 & W_{i,j,k} < 3.5002 \text{ m/s or } W_{i,j,k} > 30 \text{ m/s} \\ 807.69 + W_{i,j,k} \left( -495.51 + W_{i,j,k} (77.88 - 0.64 W_{i,j,k}) \right) & 3.5002 \leq W_{i,j,k} \leq 10 \text{ m/s} \\ 12,800 + W_{i,j,k} \left( -5713.3 + W_{i,j,k} (740.0 - 26.667 W_{i,j,k}) \right) & 10 < W_{i,j,k} \leq 13 \text{ m/s} \\ 5000 & W_{i,j,k} > 13 \text{ m/s} \end{cases} \quad (S4)$$

based on manufacturer-provided power output versus wind speed, where  $\rho_{a,STP}=1.225 \text{ kg/m}^3$  is air density at standard temperature and pressure and  $\rho_a(T,P,q)$  is air density at the current temperature ( $T$ ), pressure ( $P$ ), and specific humidity ( $q$ ). The power curve indicates a cut-in wind speed of 3.5 m/s, a cut-out wind speed of 30 m/s, and a rated wind speed of 13 m/s.

The final kinetic energy in each grid cell is thus  $E_{Fi,j,k} = E_{Ii,j,k} - \Delta E_{i,j,k}$ . The turbine also converts some kinetic energy into turbulent kinetic energy (TKE), primarily in the vertical. This is roughly accounted for in the model since the reduction in wind speed due to the turbine results in wind shear, creating mechanical turbulence and TKE through a level 2.5 TKE closure scheme (S3). The TKE increases the turbulent diffusion coefficient for momentum, increasing the vertical transport of horizontal momentum down gradients (and reducing it up gradients) in a second-order local closure calculation used in the model. Energy, moisture, and trace chemicals are similarly transported across gradients due to turbulent diffusion. No treatment of constructive or destructive interference by wakes is introduced since wakes are not resolved at the scale of interest.

The change in total kinetic energy in the grid cell is next partitioned proportionately among the kinetic energies of the surrounding  $u$  and  $v$  points with

$$\begin{aligned} E_{Fi-1/2,j,k} &= E_{Ii-1/2,j,k} E_{Fi,j,k} / E_{Ii,j,k} \\ E_{Fi+1/2,j,k} &= E_{Ii+1/2,j,k} E_{Fi,j,k} / E_{Ii,j,k} \\ E_{Fi,j-1/2,k} &= E_{Ii,j-1/2,k} E_{Fi,j,k} / E_{Ii,j,k} \\ E_{Fi,j+1/2,k} &= E_{Ii,j+1/2,k} E_{Fi,j,k} / E_{Ii,j,k} \end{aligned} \quad (S5)$$

The final wind speed at each  $u$  and  $v$  point is then

$$\begin{aligned}
u_{Fi-1/2,j,k} &= \text{sign}\left(\sqrt{2E_{Fi-1/2,j,k}/M_{i-1/2,j,k}}, u_{i-1/2,j,k}\right) \\
u_{Fi+1/2,j,k} &= \text{sign}\left(\sqrt{2E_{Fi+1/2,j,k}/M_{i+1/2,j,k}}, u_{i+1/2,j,k}\right) \\
v_{Fi,j-1/2,k} &= \text{sign}\left(\sqrt{2E_{Fi,j-1/2,k}/M_{i,j-1/2,k}}, v_{i,j-1/2,k}\right) \\
v_{Fi,j+1/2,k} &= \text{sign}\left(\sqrt{2E_{Fi,j+1/2,k}/M_{i,j+1/2,k}}, v_{i,j+1/2,k}\right)
\end{aligned} \tag{S6}$$

where  $\text{sign}()$  indicates that the sign of the final scalar velocity needs to be that of the initial value. Since each  $u$  and  $v$  point borders two grid cells, it is necessary to ensure that all grid cells are solved independently with initial wind speeds and that final  $u$  and  $v$  wind speeds at each border point are determined by adding differences from Equation S6, such as  $u_{Fi-1/2,j,k} - u_{i-1/2,j,k}$  for both adjacent cells to the initial value,  $u_{i-1/2,j,k}$ , to obtain the final wind speed at the border point.

Energy conservation due to power generation and frictional dissipation of winds at the surface is maintained in the model by converting all electric power generated by the wind turbines to heat. The model also converts kinetic energy lost by natural surface roughness to turbulence and then heat. The electric power generated by turbines each time step,  $\Delta E_{i,j,k}$ , modifies the surface air temperature (where the electric power is consumed by human activity). Since the global model grid cells for the present simulations are large, it is assumed that the electricity is consumed in the same column that it is generated in. The temperature change (K) during a time step in surface layer  $ksfc$  due to electric power extraction in the model layers  $k$  between the bottom and top of a turbine rotor is

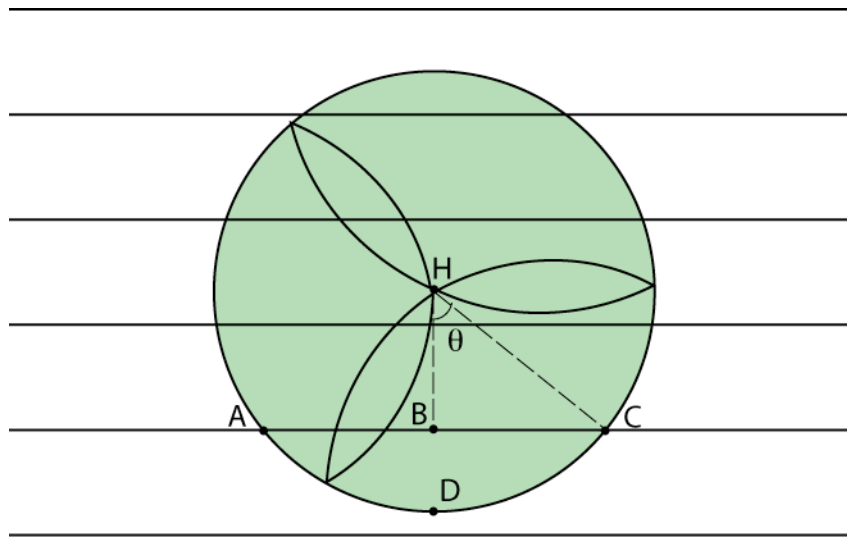
$$\Delta T_{i,j,ksfc} = \frac{1}{c_{p,m} M_{i,j,ksfc}} \sum_{k=\text{bottom}}^{\text{top}} \Delta E_{i,j,k} \tag{S7}$$

where  $c_{p,m}$  is the specific heat of moist air at constant pressure. Similarly the  $u$ - and  $v$ -components of kinetic energy lost due to friction and TKE generation at the topographical surface each time step are converted to internal energy and added to the temperature in the bottom model layer.

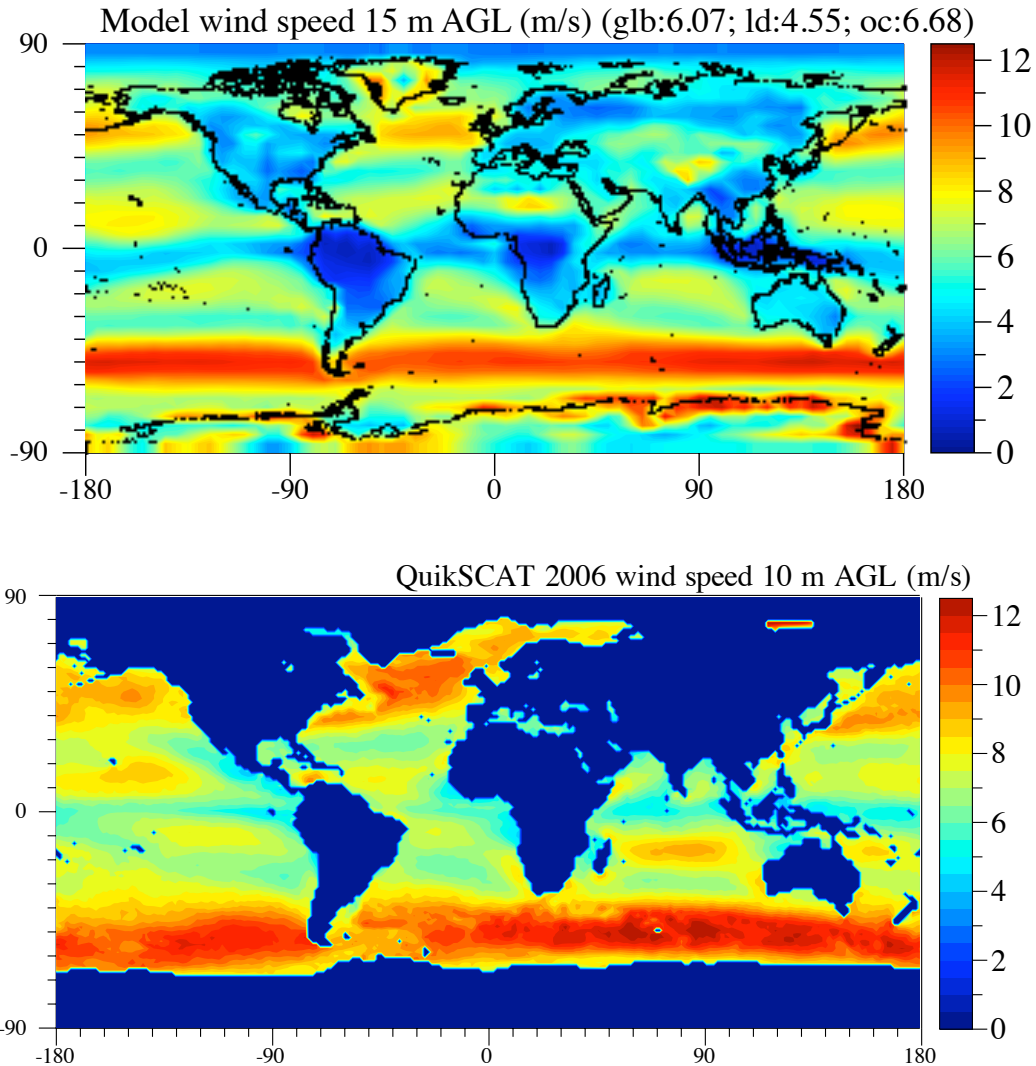
The model was initialized with  $1^\circ \times 1^\circ$  reanalysis meteorological fields (*S4*) for simulations starting January 1, 2006 and run forward in time with no data assimilation, as described in the main text.

### Supporting Figures

**Figure S1.** Illustration of how the swept area of a single wind turbine intersects multiple model vertical layers in a single grid column. Points A, B, C, D, and H are discussed in the text.

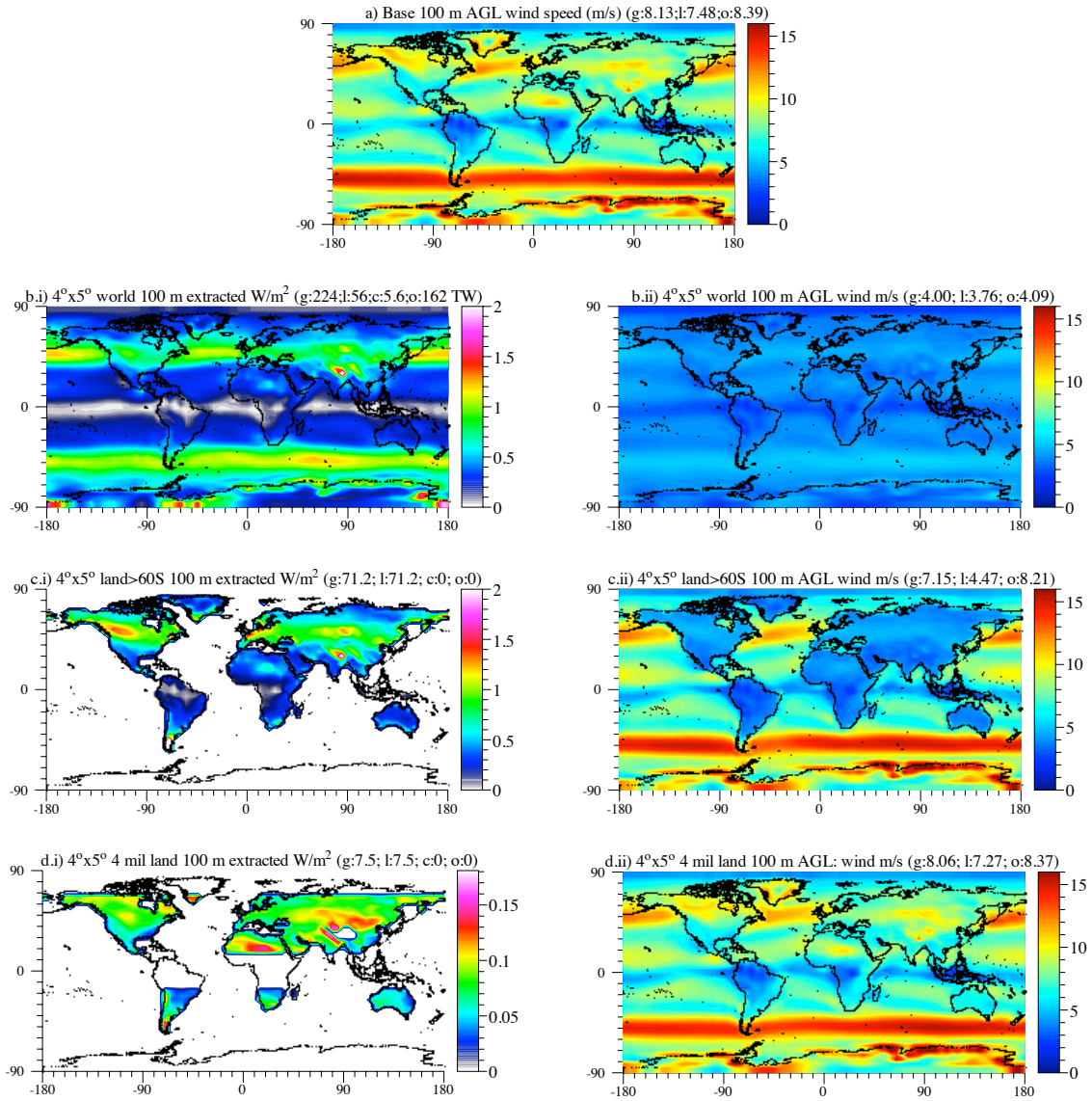


**Figure S2.** Modeled 2006 15-m wind speed at 4x5 degree resolution versus 10-m data (S5) for the same year.



**Figure S3.** (a) Modeled ( $4^{\circ}\times 5^{\circ}$  horizontal resolution) annually-averaged (during the last year of simulation) 100-m wind speeds in the absence of wind turbine power extraction (Simulation A). (b) Same as (a) but for power ( $\text{W}/\text{m}^2$ ) extracted from wind turbines (left) and the resulting wind speeds (m/s) (right) accounting for worldwide turbine momentum extraction (Simulation B). (c) Same as (b) but for wind turbines over all land outside Antarctica (Simulation I). (d-f) Same as (b) but for the three cases of 4 million turbines

(Simulation N-P), (g) Same as (b) but for turbine extraction in the jet stream at 10 km (Simulation Q). g=global average; l=land-average; c=coastal ocean (water with depth less than 200 m outside Antarctica) average, and o=all other ocean average.



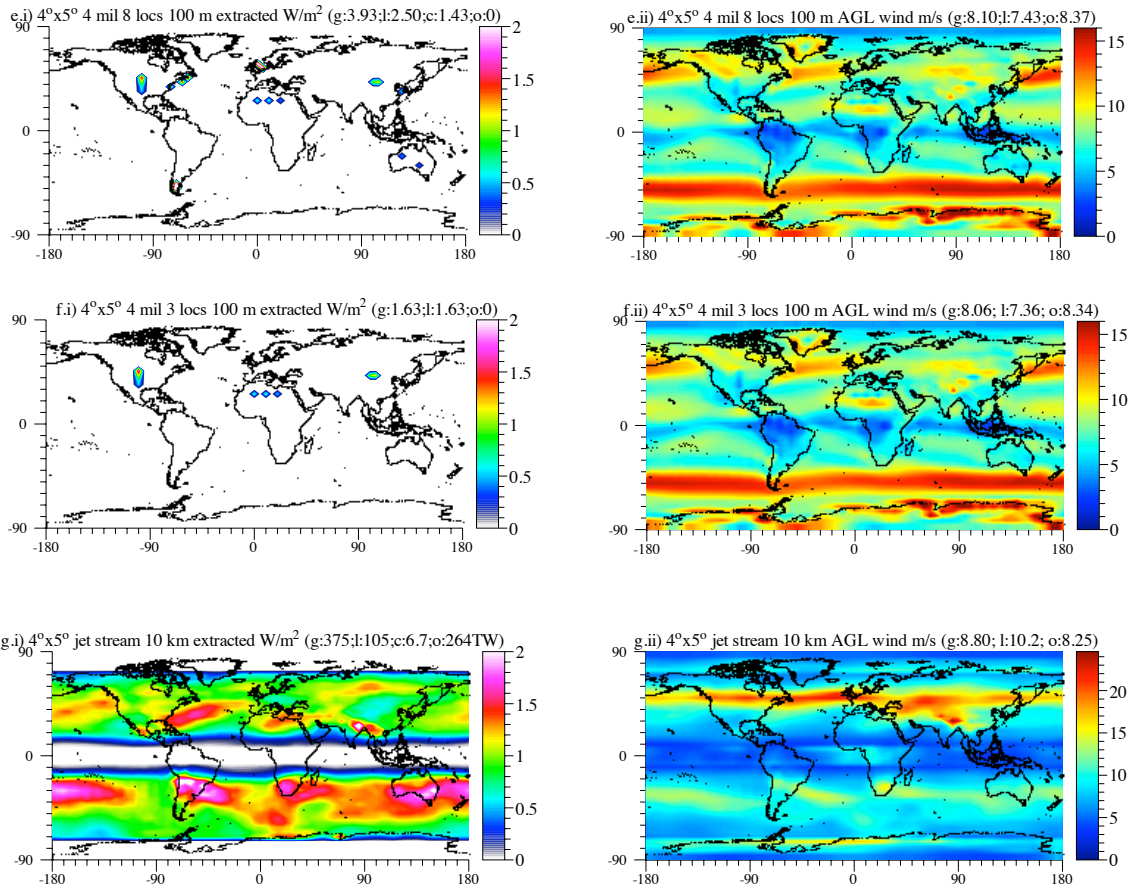


**Figure S4.** Zonally-averaged changes during the last simulation year in several meteorological variables between the global surface turbine case (Simulation B) and the base case.

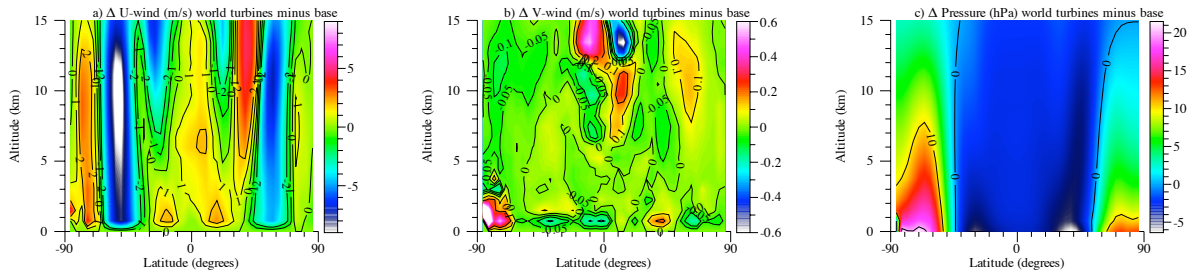
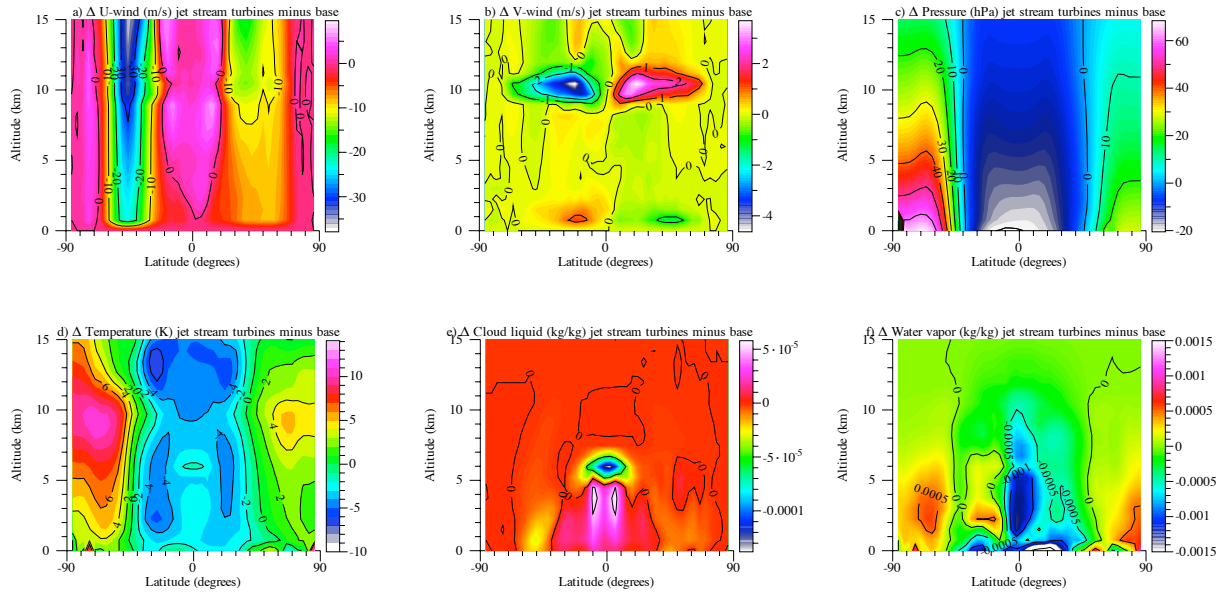


**Figure S5.** Zonally-averaged changes during the last simulation year in several meteorological variables between the case with turbines at 10 km (jet stream case, Simulation Q) and the base case.



### Supporting References and Notes

- S1. M.Z. Jacobson, *J. Geophys. Res.* **106**, 5385 (2001).
- S2. G.M. Masters, *Renewable and efficient electric power systems*, John Wiley & Sons, Hoboken, NJ (2004).
- S3. G.L. Mellor, T. Yamada, *Rev. Geophys. Space Phys.* **20**, 851 (1982).
- S4. Global Forecast System (GFS), <http://nomads.ncdc.noaa.gov/data/gfs-avn-hi/> (2010), Accessed February 23, 2012.
- S5. Quikscat, [http://podaac.jpl.nasa.gov/DATA\\_CATALOG/quikscatinfo.html](http://podaac.jpl.nasa.gov/DATA_CATALOG/quikscatinfo.html) (2010), processed by Dan Whitt and Mike Dvorak, Accessed February 23, 2012.